Biochimica et Biophysica Acta, 501 (1978) 33—52
© Elsevier/North-Holland Biomedical Press

BBA 47431

THE STRUCTURE OF A CYTOCHROME OXIDASE-LIPID MODEL MEMBRANE

J.K. BLASIE, M. ERECIŃSKA, S. SAMUELS and J.S. LEIGH

Department of Biochemistry and Biophysics, School of Medicine, University of Pennsylvania, Philadelphia, Pa. 19174 (U.S.A.)

(Received May 3rd, 1977)

Summary

The structure of "membranous cytochrome oxidase" has been investigated by X-ray diffraction, optical polarization spectroscopy and EPR spectroscopy. These studies indicate that the cytochrome oxidase molecules are oriented asymmetrically in the membrane profile with a significant portion of their mass occurring within the extravesicular surface of the membrane; the oxidase molecultes span the membrane profile; the distribution of the oxidase molecules over the plane of these membranes is non-crystalline; the oxidase molecules contain bundles of α-helical polypeptide chain segments where the average orientation of the helices is normal to the membrane plane; and the average heme orientation within the oxidase molecules is such that the normal to the heme plane lies in the plane of the membrane.

Introduction

Cytochrome *c* oxidase, tightly bound to the mitochondrial inner membrane, transfers reducing equivalents from cytochrome *c* to molecular oxygen with the formation of water and simultaneous synthesis of ATP. This protein, with molecular weight of approx. 120 000 [1], is composed of at least five polypeptide chains [1—4] and contains four one-electron redox components: two hemes and two copper atoms. The two hemes are functionally distinct (for summary see refs. 5 and 6): one, heme a_3, reacts with oxygen and other ligands, the other, heme *a*, reacts with reduced cytochrome *c*.

The activity of the enzyme depends on its interaction with detergents [7] or lipids [8]. When isolated from its native environment, it contains certain amounts of lipid and some preparations termed "membranous cytochrome oxidase" [9] spontaneously form membrane-bounded vesicles in which a fraction of the total phospholipid is bound to the hydrophobic surface of the oxidase-

protein complex [10]. The planar organization of the oxidase molecules appears to be crystalline over the plane of the membranes in certain preparations of such "membranous cytochrome oxidase" [11]. Electron diffraction and electron microscopy of such crystalline lattices of the oxidase have been recently used to provide an approximate low-resolution three-dimensional electron density distribution for the negatively stained molecule [12].

Freeze-fracture electron microscopy studies of reconstituted lipid membrane vesicles which contain active oxidase revealed the presence of particles on the fracture faces of freeze-fractured membranes [13] and suggested that those particles span the lipid bilayer. Evidence has accumulated that in the mitochondrial membrane the oxidase also spans the inner membrane [14—18].

Previous attempts to detect orientation of cytochrome oxidase within the mitochondrial membrane have utilized the method of photoselection and linear dichroism [19] and have suggested that cytochrome oxidase is either completely immobilized within the mitochondrial membrane or that it rotates about a single axis such that the plane of the a_3 heme is parallel to the plane of the mitochondrial inner membrane.

In this paper, we have used X-ray diffraction methods applied to hydrated oriented multilayers of "membranous cytochrome oxidase" in order to determine the distribution and structure of the oxidase molecule in the membrane profile and its distribution in the membrane plane. In addition we have obtained X-ray diffraction data arising from the secondary and tertiary structure of the oriented oxidase molecules in these multilayers. We have also used polarized optical absorption and EPR spectroscopy on these same oriented multilayers in order to determine the orientation of the two heme chromophores of the oxidase relative to the plane of this model membrane. This work has been briefly reported previously [20].

Methods

(1) Preparation of the "membranous cytochrome oxidase". "Membranous cytochrome oxidase" was purified from pigeon breast mitochondria (isolated by the method described previously [21]) which were stored frozen at −50°C. The thawed mitochondria were diluted 10-fold by the addition of 0.01 M phosphate buffer at pH 7.2 and centrifuged for 10 min at 10 000 × *g*. The pellet was washed once in 0.1 M phosphate buffer, pH 7.2, and suspended in 0.25 M sucrose/0.01 M phosphate buffer, pH 7.4, at a protein concentration of 30 mg/ml. A 10% aqueous solution of Triton X-114 was then added to the suspension to produce 0.5 mg detergent/mg of mitochondrial protein, followed by the addition of solid KCl to give an 0.2 M final concentration. The mixture was allowed to stand for 20 min at 4°C and at the end of the incubation period was centrifuged at 100 000 × *g* for 40 min. The clear supernatant and a small, tightly packed, dark-brown residue at the bottom of the pellet were discarded and the upper, loosely packed layer of the pellet was collected, gently rehomogenized in 5—6 times the original volume of sucrose/phosphate medium, and centrifuged for 45 min at 100 000 × *g*. The pellet was suspended in the same medium with the protein concentration adjusted to 30 mg/ml and treated with 10% aqueous solution of Triton X-100 as described by Sun et al. [9]. In order

to obtain a preparation of high purity, the treatment with Triton X-100 at a protein concentration of 20 mg/ml was repeated twice.

Analytical procedures: Heme *a* was determined as cytochrome *a* by measuring the difference in absorption at 605 nm after the addition of dithionite vs. that at 630 nm before the addition. The millimolar extinction coefficient used in the calculation was taken to be 26.4 cm^{-1} (reduced-oxidized).

Protein was measured by the biuret reaction [22] with crystalline bovine serum albumin as a standard.

Lipid was determined essentially according to the method described by Bartlett [23]. Potentiometric titration of an anaerobic preparation was carried out as described by Wilson and Dutton [24] and Dutton [25] in the presence of 20 μM diaminodurene and 40 μM phenazine methosulfate as redox mediators. $K_3Fe(CN)_6$ was used as an oxidant and a freshly prepared solution of dithionite served as the reductant.

Polyacrylamide gel electrophoresis in the presence of sodium dodecyl sulfate was carried out as described by Laemmli [26] using 12.5% acrylamide/0.6% methylenebisacrylamide with bovine serum albumin, papain, trypsin, myoglobin and cytochrome *c* as standards.

(2) Preparation of hydrated oriented multilayers of "membranous cytochrome oxidase" for the X-ray diffraction studies. "Membranous cytochrome oxidase" (25—50 mg protein/ml) was diluted 150—200-fold with 2 mM phosphate buffer, pH 7.5, in order to reduce the detergent content of the preparation. Aliquots of the "membranous cytochrome oxidase" (0.5—0.75 mg protein) were sedimented in a demountable lucite sedimentation cell [27] onto aluminum foil at approx. 70 000 $\times g$ for 1 h. The resulting fully hydrated pellet 5 mm in diameter and approx. 0.1 mm thick adhered to the aluminum foil support. The pellet on its aluminium foil support was then firmly attached to a 1 $\times$ 1 cm glass slide which was a section of a cylindrical glass shell (tube) with a curvature of approx. 0.5 cm^{-1} and immediately introduced into a sealed vial containing an inert atmosphere at approx. 90% relative humidity at 4°C. The pellet was then subjected to slow partial dehydration at 90% relative humidity at 4°C for a period of 12—24 h. This slow dehydration process resulted in the formation of a hydrated oriented multilayer of the "membranous cytochrome oxidase" (see Results) with a final water content of approx. 25% by weight.

(3) Preparation of hydrated oriented multilayers of "membranous cytochrome oxidase" for the polarized optical absorption and EPR spectroscopy. Hydrated oriented multilayers of "membranous cytochrome oxidase" were prepared for the spectroscopic studies in a manner entirely analogous to that described above for the X-ray diffraction studies except that planar glass and Mylar supports were used, respectively, for the optical and EPR spectroscopy and the diameter of the multilayer formed on Mylar supports was 1.0 cm using 5—7 mg protein.

(4) X-ray diffraction methods. The X-ray source was an Elliott GX-6 rotating anode X-ray generator generally operating at 30—35 kV and 30—40 mA. Ni-filtered CuKα radiation (λ = 1.54 Å, the α_1 and α_2 CuK lines being unresolved) was then either singly or doubly reflected from one or two curved Frank's mirrors (glass) at grazing angles of incidence up to the critical angle and thereby focused in the plane of detection into a line or a spot. Two pairs of guard slits

(vertical and horizontal) removed the unreflected beam(s), reduced parasitic scatter from the mirrors, and determined the height of the singly focused line. The beam size at the guard slits was typically 250 μm × 750 μm for the line-focus and 150 μm × 150 μm for the point-focus. The line-focused beam flux was typically $5 \cdot 10^7$ photons/mm^2 per s as measured with a position-sensitive X-ray detector [28,29].

The aluminum specimen chamber was cooled with water circulating through interior channels and the temperature was controlled to ±0.2°C. The hydrated oriented multilayer was mounted in the chamber such that the normal to the cylindrically curved multilayer surface and the cylinder axis were both perpendicular to the beam axis with the narrower beam dimension parallel to the multilayer surface; maintaining this multilayer specimen-beam geometry, the multilayer surface was then positioned to intersect the incident X-ray beam at grazing incidence resulting in a 10—20% attenuation of the incident beam caused primarily by the specimen support's intersection with the beam. The specimen chamber was sealed with a mylar entrance window and an aluminum foil exit window allowing X-rays to transverse the chamber. The hydration state of the multilayer was determined and maintained in the chamber through the use of a small reservoir of an appropriate saturated salt solution positioned immediately below the multilayer and a flow of moist He at the same relative humidity as that produced by the saturated salt solution (75—95% relative humidity was routinely used).

The X-ray diffraction from the hydrated oriented multilayers was obtained on Ilford type G X-ray film contained in a cylindrical cassette at a specimen-film distance of 62.5 mm in exposures of 18—36 h in order to record the intermediate and higher-angle regions of the diffraction pattern and in a flat-plate cassette at a specimen-film distance of 250 mm in 12—48 h exposures in order to record the low-angle diffraction. The X-ray beam path from the Frank's mirror to the point of detection on film was in vacuo.

The total lamellar X-ray diffraction obtained from these hydrated oriented multilayers of "membranous cytochrome oxidase" (which occurs along an axis parallel to the normal to the multilayer surface) was converted to digital total relative lamellar intensity data as a function of $(2 \sin \theta)/\lambda$ where 2θ is the scattering angle using a Joyce-Loeble MK-IIICS microdensitometer. The slit height used to scan along the lamellar axis of the diffraction patterns was always considerably smaller than the height (arc length or mosaic spread) of the lamellar diffraction maxima arising from the mosaic nature of the multilayer. The shape of the lamellar background scattering from the cytochrome oxidase multilayers was estimated from the shape of the scattering curve obtained along the lamellar axis from blank cylindrically curved aluminum foil-glass supports and the shape of the non-Bragg lamellar scattering obtained from highly ordered lecithin multilayer specimens and subtracted from the total lamellar intensity data. The curvature of the multilayer induced by the curvature of its aluminum foil support is sufficient to bring lamellar diffraction from a perfectly oriented multilayer (i.e. 0° mosaic spread) for $(2 \sin \theta)/\lambda < 1/5$ Å onto the Ewald sphere of reflection.

(5) Polarized optical spectroscopy methods. The hydrated oriented multilayer specimens for the optical spectroscopy were sealed at a defined water

content with a glass cover-slip and fast-curing epoxy glue. Optical contact, however, occurred only on the glass substrate side of the multilayer which therefore always faced the incident light beam in these experiments. The optical spectra in the range of 350—800 nm were recorded for incident light polarized either vertically or horizontally in the laboratory frame. An angle of incidence between the incident light beam and the normal to the plane of the multilayer support in the range 0°—60° was generated by rotation of the multilayer about an axis lying in the plane of the multilayer substrate which was vertical in the laboratory frame (see ref. 30 for further details).

The optical spectra were recorded from the hydrated "membranous cytochrome oxidase" multilayers on a Cary 14 split-beam spectrophotometer as a function of incident beam polarization utilizing matched polarizers (Polacoat 105.UV.WRMR) in the measuring and reference beam and a lipid multilayer of comparable optical thickness in the reference beam for 0°, 45° and 60° angles of incidence. For some experiments, matched analyzers were placed in the measuring and reference beams transmitted by the two multilayer specimens and spectra were similarly recorded for parallel and perpendicular polarizer-analyzer orientations.

Optical spectra were also recorded using a scanning dual-wavelength spectrophotometer designed and constructed in the Johnson Foundation shops which was interfaced with a PDP-11/10 computer. The optical spectra were recorded on this device from hydrated "membranous cytochrome oxidase" multilayers as a function of incident beam polarization for 0° and 45° angles of incidence. The reference wavelength was chosen at 650 nm and reference spectra were generated by allowing the light beam to transverse the sealed glass support-multilayer-glass coverslip specimen in regions immediately adjacent to the multilayer itself for the corresponding beam polarizations and angles of incidence. In addition, similar spectra were obtained as a function of beam polarization at a 45° angle of incidence where the sealed glass support-multilayer-coverslip specimen was placed in a 1 cm path-length cuvette (whose windows were at normal incidence to the beam) containing media of various refractive indices.

(6) EPR spectroscopy methods. For the EPR measurements, the hydrated oriented cytochrome oxidase multilayer together with its supporting mylar support was cut into 2 × 10 mm strips which were inserted inside a 3 mm internal diameter quartz EPR tube in such a way that the planes of the supporting mylar supports were parallel to one another. The samples were frozen by immersion of the tubes in liquid N_2 and the spectra recorded at approx. 10°K using a Varian E-109 spectrometer equipped with an Air Products LTD-3-110 liquid helium cryostat and a PDP-11/10 computer. The tubes were marked such that spectra could be recorded with the applied magnetic field oriented either parallel or normal (perpendicular) to the planes of the mylar supports.

Results

(1) Characteristics of the "membranous cytochrome oxidase"

The preparation of "membranous cytochrome oxidase" obtained as described in Methods contained heme *a* at a concentration of 12—14 nmol/mg protein and approx. 20% lipid (w/w). The oxidized preparation exhibited absorption

maxima at 598 and 421 nm, while those of the reduced preparation were at 603 and 444 nm. The potentiometric titration of an anaerobic preparation of the oxidase revealed the presence of two components with half-reduction potentials at pH 7.2 and 22°C of 0.375 V and 0.23 V. Polyacrylamide gel electrophoresis in sodium dodecyl sulfate showed the presence of five bands with molecular weights of 38 000, 24 000, 14 000, 12 000, and 9000.

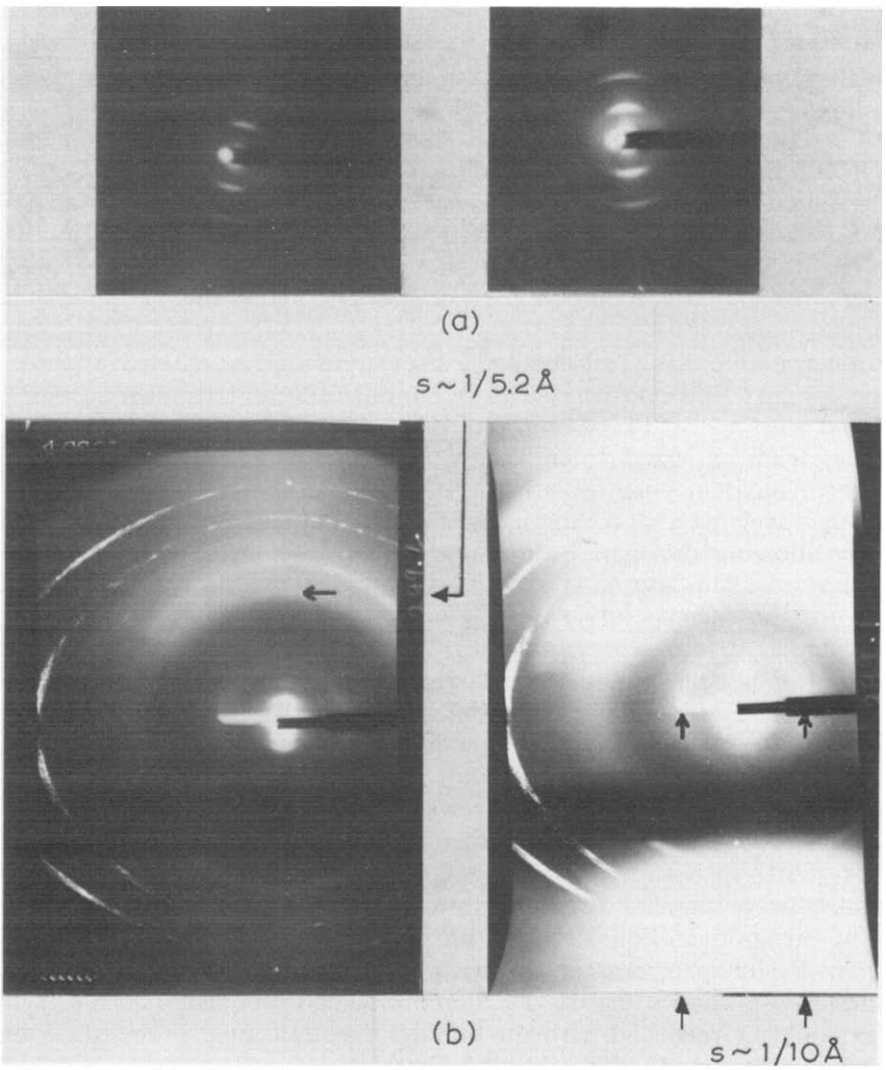

Fig. 1. Low-angle (a) and intermediate and high-angle (b) regions of the X-ray diffractive pattern from a hydrated oriented multilayer of "membranous cytochrome oxidase" at 90% relative humidity at 4°C obtained with the flat-plate and cylindrical cassettes, respectively, and line-focus beam as described in Methods. The lamellar (meridional) diffraction occurs approximately along the vertical axes in this figure. In a, the stronger lamellar reflections occur at $s \simeq h/D$ for h = 2, 4 and 6 and $D = \simeq 156$ Å. In b, higher-angle lamellar diffraction is observable extending out to $s \approx 1/8$ Å; a strong meridional component is indicated by the arrow in this diffraction pattern at $s \approx 1/5.2$ Å and the equatorial diffraction possesses strong components in the region $s \approx 1/10$ Å as indicated by the arrows. The lower half of these diffraction patterns is attenuated by absorption in the multilayer and its support.

(2) Nature of the X-ray diffraction patterns

The low-angle and the intermediate and high-angle regions of the X-ray diffraction pattern from hydrated oriented multilayers of "membranous cytochrome oxidase" at 90% relative humidity and 4°C obtained with the flat-plate and cylindrical cassettes, respectively, and line-focus beam are shown in Fig. 1. Characteristic lamellar meridional diffraction from the multilayer occurs along the vertical axes in this figure and the beam is focused for diffraction along this axis. The lamellar diffraction has a mosaic spread of 10—15° (full width at half-maximum) as determined from the degree of arcing in the lamellar diffraction maxima. The lamellar diffraction has relatively sharp maxima at lower-angle which monotonically increase in width toward increasingly higher-angles indicating the presence of lattice disorder [31] within the multilayer as shown in Fig. 3. The stronger lower-angle lamellar diffraction maxima (all of which have linewidths greater than the focused-beam linewidth) occur at $s \simeq h/D$ for h = 2, 4 and 6 and $D \simeq 156$ Å where $s = (2 \sin \theta)/\lambda$ and D is the periodicity of the multilayer lattice. Much weaker low-angle lamellar diffraction maxima occur at

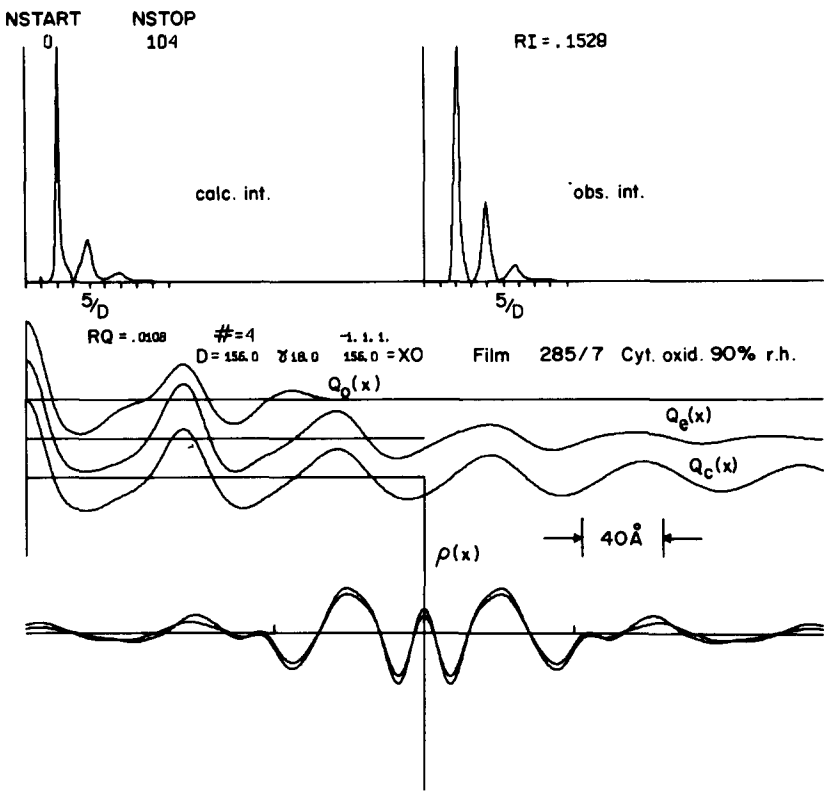

Fig. 2. Some of the functions utilized in the Generalized Fourier Synthesis Deconvolution Method analysis to derive the most-probable low-resolution (≈20 Å) unit cell electron density profile $\rho(x)$. The tick marks on the abscissa in $\rho(x)$ denote the locations $x = \pm D/2$ where $D = 156$ Å. The 40 Å dimension marker applies to $\rho(x)$, its autocorrelation function $Q_0(x)$ and the experimental and calculated Q functions $Q_e(x)$ and $Q_c(x)$, respectively. The "obs. int." function shown is the experimental intensity function $I_e(s)$ where $s = h/D$ is denoted on the abscissa for $h = 1, 2, 3, \ldots$

$s \simeq h/D$ for $h = 1$, 3 and 5 which become somewhat stronger at other multilayer periodicities produced by other relative humidity atmospheres for the multilayer. The observable lamellar diffraction in these experiments usually extends continuously out to $s \approx 1/8$ Å. An additional relatively strong meridional diffraction maximum is observed at $s \approx 1/5.2$ Å.

The equatorial diffraction from the hydrated cytochrome oxidase multilayer occurs along the horizontal axes in Fig. 1 and is not sharpened substantially when a point-focus beam is used. The equatorial diffraction is characterized by weak diffuse maxima at lower and intermediate diffraction-angles and possesses strong broad components in the region of $s \approx 1/10$ Å whose mosaic spread (degree of arcing) is somewhat greater than that of the lamellar diffraction. Strong broad equatorial diffraction also occurs in the $s \approx 1/4.6$ Å region which shows considerably greater mosaic spread than that of the lamellar diffraction.

These X-ray diffraction patterns described are characteristic of 20 multilayer specimens investigated. The patterns are of course invariant to rotation of the specimen about the normal to the multilayer plane. The multilayer periodicity D has been varied over a 154—170 Å range using specimen atmospheres of 81—95% relative humidity.

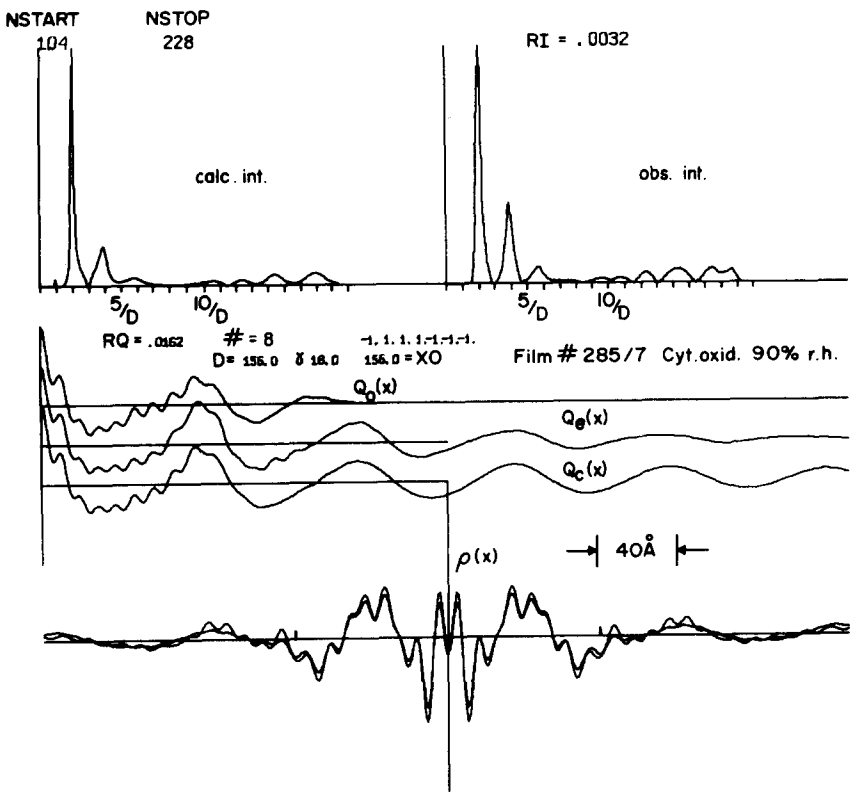

Fig. 3. Some of the functions utilized in the Generalized Fourier Synthesis Deconvolution Method analysis to derive the "tentative" high-resolution (≈8 Å) unit cell electron density profile $\rho(x)$. The abbreviations and denotations are the same as those in Fig. 2.

Analysis of the lamellar X-ray diffraction patterns

The background corrected lamellar X-ray intensity data must be corrected by a factor of s^2 in order to obtain the lamellar intensity function $I_e(s)$. One factor of s arises from the intersection of the Ewald sphere of reflection with the reciprocal lattice for the oriented multilayer (Lorentz correction) and the other factor of s is an approximate microdensitometry correction arising from scanning the lamellar reflections with a slit of relatively short height compared to the mosaic spread (degree of arcing) of the lamellar diffraction maxima. This latter approximate correction has recently been shown to be valid [29] for such beam-specimen geometries and these degrees of mosaic spread. The complete corrected lamellar intensity function $I_e(s)$ is shown in Fig. 3 for the multilayer at 90% relative humidity and 4°C (the relatively weak maxima at s = 1, 3 and $5/D$ have been omitted in this figure).

An analysis of this lamellar intensity function can provide under appropriate conditions the electron density profile for one unit cell in the multilayer lattice. The unit cell electron density profile represents a projection of electron density along the planes of the membranes within one unit cell of the oriented multilayer onto an axis normal to these planes, the profile axis [32]; the unit cell profile has an extension D along this axis. Hence, the unit cell electron density profile arises from the average distribution of membrane components in the membrane profile (or cross-section).

The analysis which we shall apply to the lamellar intensity function is the Generalized Fourier Synthesis Deconvolution Method described in detail previously [31]. We shall only briefly highlight the method as applied to the lamellar intensity function for the hydrated oriented cytochrome oxidase multilayers liberally referring to the earlier paper.

The Patterson function for an oriented membrane multilayer lattice exhibiting lattice disorder, termed the experimental Q function $Q_e(x)$, is calculated directly from the lamellar intensity function $I_e(s)$ according to Eqn. 1:

$$Q_e(x_j) = 2 \sum_{k=1}^{N_k} I_e(s_k) \cdot s_k^2 \cos(2\pi x_j s_k) \cdot \Delta s$$

$$x_j = j\Delta x \qquad \Delta x = 1\,\text{Å} \qquad N_k = \text{total number of data points in } I_e(s_k)$$

$$s_k = k\Delta s \qquad \Delta s = (1925\,\text{Å})^{-1} \tag{1}$$

$Q_e(x_j)$ closely approximates $Q_e(x) = \mathcal{F}^{-1}(I_e(s))$ where $\mathcal{F}$ denotes the Fourier transform operator when Δs (the digitization interval for $I_e(s)$) is sufficiently small that $I_e(s)$ is essentially constant within the interval Δs. In this analysis, Δs = (1925 Å)$^{-1}$. The experimental Q function corresponding to the $I_e(s)$ in Fig. 3 is also shown in Fig. 3. $Q_e(x)$ is pseudoperiodic in D (=156 Å in this case) as supported by the fact that the fine-structure in $Q_e(x)$ about the origin extends throughout the region $0 \leq x \leq D$ as expected for lattice-disordered multilayers [31] necessarily consistent with the sampling interval of the low-angle lamellar diffraction maxima in reciprocal space.

The analysis developed by Schwartz et al. [31] allows the identification of the autocorrelation function of the unit cell electron density profile for the

multilayer in $Q_e(x)$ and its subsequent deconvolution to provide the unit cell electron density profile itself. The analysis produces a calculated Q function, $Q_c^{(k)}(x)$ for the k^{th} phase combination. Since there are eight zeroes in the experimental intensity function $I_e(s)$ (where the total lamellar diffraction approaches the estimated background lamellar scattering to within experimental errors) as shown in Fig. 3, these zeroes define seven regions of constant phase * within the lamellar intensity function and there exist in principle 2^6 possible phase combinations. The calculated $Q_c^{(k)}$ functions for the various phase combinations were compared quantitatively with the experimental $Q_e(x)$ function. The residual R_Q for the Q function fit was calculated according to the following equation from Schwartz et al. [31] for the k^{th} phase combination.

$$R_Q^{(k)} = \frac{\sum_{j=1}^{N_j} (Q_e(x_j) - Q_c^{(k)}(x_j))^2}{\sum_{j=1}^{N_j} (Q_e(x_j))^2} \tag{2}$$

The resulting $R_Q^{(k)}$ values for the various phase combinations are then ranked, the minimal $R_Q^{(k)}$ corresponds to that phase combination representing the most probable unit cell electron density profile while the maximal $R_Q^{(k)}$ corresponds to that phase combination representing the least probable profile. Hence, the analysis generates a hierarchy of most probable unit cell electron density profiles; the ultimate identification of the most probable unit cell electron density profile as the uniquely correct profile depends upon whether the $R_Q^{(k)}$ for the most probable profile is significantly different from the $R_Q^{(k)}$ for the second most probable profile (and so on down the hierarchy) in the statistical sense which depends directly upon the statistical accuracy of the lamellar intensity function. The reader is referred to Schwartz et al. [31] for a complete discussion of the theoretical validity of the analysis for generating this hierarchy of most probable profiles. The more probable unit cell electron density profiles are then calculated from Eqns. 13 and 14 in Schwartz et al. [31].

Specifically for the lamellar intensity function shown in Fig. 3, the values of γ (the lattice disorder parameter) and D were refined until the amplitude and shape of the maximum in the calculated $Q_c^{(k)}(x)$ functions at $x \approx 156$ Å matched that in $Q_e(x)$ as closely as possible; this occurred for $D = 156$ Å and $\gamma = 18.0$ Å. The entire lamellar intensity function extending out to $s \approx 1/8$ Å was

* Inasmuch as the multilayers were formed from a relatively homogeneous population of membranous cytochrome oxidase vesicles, we expect the unit cell of the multilayer to contain the membrane pair corresponding to one flattened vesicle which would contain a mirror plane of symmetry in the profile projection between the two membranes of the pair causing the unit cell profile projection to contain a center of symmetry; hence these regions between the zeroes would be of constant phase of 0 or π only. The relatively large periodicities ($154 \leq D \leq 170$ Å) and relatively low water contents of the hydrated multilayers support this conclusion regarding the contents of the unit cell. In addition, the studies of Henderson et al [12] on crystalline forms of "membranous cytochrome oxidase" also support this conclusion.

used in this refinement. Inasmuch as the considerably more intense lamellar intensity function maxima for $s \leq 8/D$ dominate the $Q_e(x)$ function and since they also have higher statistical accuracy, the analysis was first applied to the lamellar intensity function for $s \leq 8/D$. The resulting hierarchy of $R_Q^{(k)}$ values for the four possible phase combinations at this resolution showed that the phase combination π, 0, 0 for the first three maxima of the lamellar intensity function most probably had an $R_Q^{(k)}$ value less than half that of the next most probable phase combination. The corresponding most probable unit cell electron density profile $\rho_0(x)$ is shown in Fig. 2 for the region $-D/2 \leq x \leq +D/2$ along with the $Q_e(x)$ and $Q_c^{(k)}(x)$ for the π, 0, 0 phase combination at a resolution of $D/8 \approx 20$ Å. This most probable electron density profile at this resolution should certainly be the uniquely correct profile based on the statistically significantly different $R_Q^{(k)}$ values at this particular resolution; this conclusion is strengthened by the fact that three different sets of lamellar intensity function data having different D and γ values arising from different water contents in the various multilayers all generated this same most probable unit cell electron density profile under the analysis at comparable resolution.

The resolution of the analysis was then extended using the complete lamellar intensity extending out to $s \approx 1/8$ Å. Inasmuch as the third intensity maximum in the region $s \approx 6/D$ has an amplitude comparable to that of the higher-angle maxima, consideration of the Fourier sampling theorem suggested that its phase could in principle be affected by the phases of the neighboring intensity maxima at higher-angle. Therefore, only the phases of the first two intensity function maxima determined to be π, 0, respectively, in the lower resolution analysis described above were maintained fixed yielding 2^5 possible phase combinations for the higher-angle maxima for $s > 5/D$. The first few more probable phase combinations in the $R_Q^{(k)}$ hierarchy generated by the Generalized Fourier Synthesis Deconvolution Method analysis at this higher resolution were not significantly different statistically due to the lesser statistical accuracy of the higher-angle lamellar intensity data and the considerably lesser effect of this higher-angle data on the $Q_c^{(k)}(x)$ functions owing to their relatively weak amplitudes. As a result, the most probable unit cell electron density profile arising from the analysis at this higher resolution (≈ 8 Å) cannot at this stage of analysis be considered to be the uniquely correct profile. Hence, this most probable "high-resolution" profile $\rho_0(x)$ as shown in Fig. 3 for $-D/2 \leq x \leq +D/2$ shall be referred to as "tentative" in the discussion section of this paper (Fig. 3 also contains the higher-resolution $Q_c^{(k)}(x)$ for the most probable phase combination). It is interesting to note, however, that (a) the analysis at this higher resolution again indicated the phase of the third intensity function maximum at $s \approx 6/D$ to be 0 and (b) the most probable unit cell electron density profile at this higher-resolution is also the smoothest which one would expect to be a necessary requirement for the profile projection of a multicomponent membrane. Inasmuch as variation in the water content of the multilayer does not affect the nature of the higher-angle lamellar intensity function maxima due to the relative degree of lattice disorder present in the multilayers at these water contents, phasing of these maxima will have to be achieved through the use of data with higher statistical accuracy or data obtained from more highly ordered multilayer lattices.

(4) Nature of the polarized optical spectra

For an angle of 0° between the incident light beam and the normal to the plane of the glass support, the optical absorption spectra obtained with vertically and horizontally polarized light (in the laboratory frame) throughout the wavelength range 350—700 nm are essentially identical to within experimental error for the oxidized cytochrome oxidase multilayers irrespective of whether the split-beam or double-beam spectrophotometer is used to record the spectra. The spectra show features characteristic of oxidized cytochrome oxidase. This lack of difference in the spectra for the two polarizations at 0° angle of incidence indicates that the hydrated oriented multilayers of "membranous cytochrome oxidase" are cylindrically symmetrical about the normal to the plane of the multilayer in agreement with the X-ray diffraction results.

For an angle of 45° or 60° between the incident light beam and the normal to the plane of the glass support, the spectra obtained are again characteristic of oxidized cytochrome oxidase. However, the amplitude of the optical absorption spectra obtained for horizontally polarized light is greater than or equal to that obtained with vertically polarized light throughout the wavelength range 350—700 nm assuming that these two polarized absorption spectra are approximately equal in amplitude in the 700—800 nm region. This is shown in Fig. 4 using the double-beam spectrophotometer, especially in the difference spectrum represented by the dotted lines. Again, this qualitative result is similar for data obtained with both the split-beam and double-beam spectrophotometers

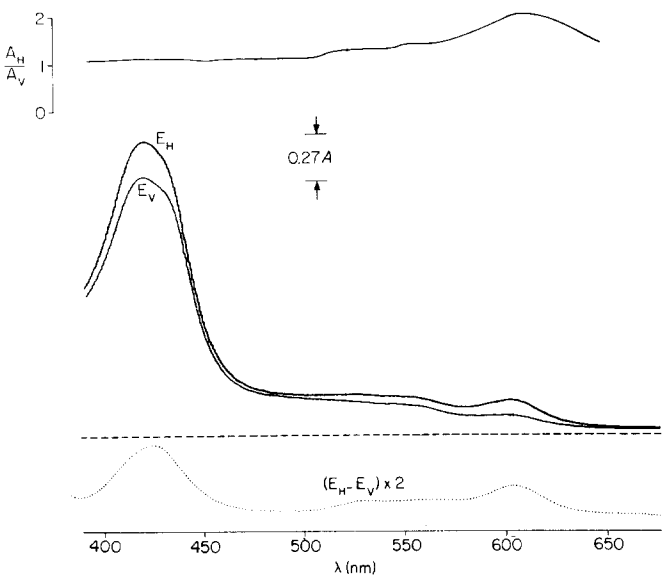

Fig. 4. Polarized optical absorption spectra of oxidized cytochrome *c* oxidase in hydrated oriented multilayers of "membranous cytochrome oxidase" recorded at an angle of 45° between the incident beam and the normal to the plane of the multilayer. The membrane multilayer was formed from 0.52 mg protein (6.3 nmol heme *a*) of "membranous cytochrome oxidase" and partially dehydrated at 4°C for 24 h at 90% relative humidity. E_H and E_V denote the horizontal and vertical polarizations of the incident light beam in the laboratory frame. The broken line represents the approximate baseline against which the polarization ratio was calculated. The dotted line is the difference spectrum.

for a minimum of ten different cytochrome oxidase multilayer specimens.

The physically relevant data are the dichroic ratios for the principal cytochrome oxidase absorption maxima, namely the Soret band at 421 nm and the α-band at 598 nm for the oxidized enzyme. The dichroic ratio is defined here as the ratio of the absorption for horizontally polarized light to that for vertically polarized light, i.e. $D(\lambda) \equiv A_H(\lambda)/A_V(\lambda)$ where $D(\lambda)$ is the dichroic ratio at a particular optical wavelength. Minimal dichroic ratios may be calculated using an approximate baseline constant in λ and equal to the absorption at $\lambda \approx 700$ nm for the two polarized optical spectra. The dichroic ratios calculated in this manner are minimal because the baseline is most likely a monotonically increasing function of λ as λ decreases from 700 to 350 nm as indicated by optical polarization spectra obtained with the split-beam spectrophotometer with a hydrated lipid multilayer in the measuring beam and only a glass support in the reference beam.

We have chosen to present the dichroic ratios calculated from polarized optical spectra obtained with the split-beam spectrophotometer because (a) the matched polarizer orientations and the matched cytochrome oxidase multilayer (measuring beam) and lipid multilayer (reference beam) orientations are known and matched to less than 0.1° and repeatable to less than 0.1° and (b) the hydrated oriented lipid multilayer in the reference beam tends to minimize the error in using the approximate baseline described above. The range of dichroic ratios for the Soret and α-bands obtained from several different cytochrome oxidase multilayers is shown below where α is the angle between the incident light beam and the normal to the multilayer's glass support.

(5) Analysis of the polarized optical spectra

The electronic transitions responsible for the Soret and α-bands in hemes are generally thought to evidence x-y equivalency, i.e. they are essentially isotropically polarized in the plane of the heme [33]. We have derived a relationship between D, the dichroic ratio, α, the angle between the incident light beam and the normal to the multilayer plane and γ_0, the angle between the normal to the heme plane and the normal to the multilayer plane, for oriented multilayers which possess cylindrical symmetry about the normal to the multilayer plane. We first consider two absorption transitions with transition moments T_1 and T_2 where θ_1 and θ_2 are the respective angles between the transition moments and the normal to the multilayer plane. If the two transitions have approximately equal energies characterized by λ, then the total absorption for incident light polarized either horizontally or vertically in the laboratory frame for the multilayer specimen-beam geometry described in Methods section 5 is given by the following expressions utilizing equations analogous to those developed by Cherry et al. [34]:

$$A_H(\lambda) = \{|T_1(\lambda)|^2 \cos^2\theta_1 \sin^2\alpha + \tfrac{1}{2}|T_1(\lambda)|^2 \sin^2\theta_1 \cos^2\alpha + |T_2(\lambda)|^2 \cos^2\theta_2 \sin^2\alpha + \tfrac{1}{2}|T_2(\lambda)|^2 \sin^2\theta_2 \cos^2\alpha\}$$

$$A_V(\lambda) = \{\tfrac{1}{2}|T_1(\lambda)|^2 \sin^2\theta_1 + \tfrac{1}{2}|T_2(\lambda)|^2 \sin^2\theta_2\} \quad (3)$$

If the two transitions T_1 and T_2 are x-y polarized heme transitions, i.e. they lie

TABLE I

$\alpha = 45°$	D (421 nm) = 1.11—1.13	D (598 nm) = 1.37—1.61
$\alpha = 60°$	D (421 nm) = 1.17—1.20	D (598 nm) = 1.50—1.97

in the heme plane at right angles to one another, and if the two transitions have equal probabilities, i.e. $|T_1|^2 = |T_2|^2$, then:

$$D(\lambda) = \left\{\frac{A_H(\lambda)}{A_V(\lambda)}\right\} = \left\{2\sin^2\alpha\left[\frac{\sin^2\gamma_0}{2-\sin^2\gamma_0}\right] + \cos^2\alpha\right\} \tag{4}$$

It is important to emphasize the latter assumption of x-y equivalency (i.e. $|T_1|^2 = |T_2|^2$) in this derivation [33]; with the assumption, the dichroic ratios reported in Table I may be used to calculate γ_0 values.

Before attempting to calculate γ_0, we should first discuss the discrepancy between the dichroic ratio of the Soret band and that of the α-band. Since both transitions are supposedly isotropically polarized in the plane of the heme, their dichroic ratios should be similar. We have obtained some experimental evidence concerning the origins of this discrepancy. They are as follows:

(a) The considerably higher absorption in the Soret band compared with the α-band would be expected to cause the incident light beam to deviate inside the multilayer from the external angle of incidence α toward 0° to a greater extent for wavelengths in the Soret region according to Snell's law (ref. 35 and Adar, F., personal communication); this deviation would of course reduce the apparent dichroic ratio of the Soret band. Using the double-beam spectrophotometer, this phenomenon has been verified qualitatively in that the dichroic ratio for the Soret band increased significantly (30—40%) while that of the α-band increased somewhat, but to a much lesser extent (3—4%) as the refractive index of the medium in the cuvette surrounding the sealed cytochrome oxidase multilayer was increased from 1.0 to 1.4.

(b) The apparent baseline absorption (due to scattered light) for the Soret region is certainly greater than that of the uncorrected approximate baseline used (namely the absorption at 700 nm) as discussed previously in Section 4 above regarding minimal dichroic ratios. A proper baseline correction would increase the dichroic ratio in the Soret region by 2—5%.

(c) Polarized optical spectra obtained from hydrated oriented multilayers of cytochrome oxidase using the split beam spectrophotometer with polarization analyzers in both the reference and measuring beams which were either parallel or perpendicular to the polarizers in the measuring and reference beams indicate that the incident light beam is depolarized by scattering to a greater extent in the Soret region as compared with the α-band region. This phenomenon would be expected at shorter wavelengths and would be accentuated in regions of high-absorption thus tending to decrease the measured dichroic ratio in such regions.

Hence, it is apparent from a—c above that the corrected dichroic ratio in the Soret region may be significantly greater than that reported in Table I. Further non-trivial experiments are now underway to either quantitatively account for

these phenomena which reduce the measured dichroic ratio or to avoid these phenomena altogether in order to determine the correct dichroic ratio for the Soret band (Adar, F., Erecińska, M. and Blasie, J.K., work in progress). At this stage in our study, we have no reason to believe that the correct dichroic ratio for the Soret band is significantly different from that of the α-band. Since the α-band is affected to a much lesser extent by these phenomena due to its considerably lesser absorption in these multilayers, a calculation of γ_0 will be based on the dichroism of the α-band.

For the range of dichroic ratios reported in Table I the inversion of Eqn. 4 provides $\gamma_0 = 72°$—$90°$. (We note that there is a direct correspondence for the ranges of dichroic ratios for the two angles of incidence α, i.e. for the α-band, $D = 1.37$ at $\alpha = 45°$ and 1.50 at $\alpha = 60°$ at the lower extremes and $D = 1.61$ at $\alpha = 45°$ and 1.97 at $60°$ at the upper extremes.) If we assume a gaussian model for the mosaic spread of these oriented multilayers (i.e. a gaussian distribution for the orientations of the normals to the planes of the multilayer "crystallites" about the average orientation normal to the plane of the multilayer's glass support with a 1/e width of σ), we can simply derive the following expression for $\bar{D}$, the dichroic ratio for hemes in a mosaic multilayer where $\bar{\gamma}$ is the average angle between the heme plane normal and the normal to the multilayer's glass support:

$$\bar{D}(\lambda) = \left\{ 2\sin^2\alpha \left[\frac{\int_0^{\pi/2} P(\gamma)\sin^2\gamma d_\gamma}{\int_0^{\pi/2} P(\gamma)[2-\sin^2\gamma]d_\gamma} \right] + \cos^2\alpha \right\} \tag{5}$$

where

$$P(\gamma) = \left\{ e^{-(\gamma-\bar{\gamma})^2/\sigma^2} \Big/ \int_0^{\pi/2} e^{-(\gamma-\bar{\gamma})^2/\sigma^2} d_\gamma \right\}$$

The expression for $D(\lambda)$ given in Eqn. 4 is then the dichroic ratio for an ideal multilayer with no mosaic spread, i.e. $\sigma = 0$, where $[\bar{\gamma}]_{\sigma\to 0} = \gamma_0$. In Fig. 5, we have plotted $\bar{D}(\lambda)$ as a function of $\bar{\gamma}$ for varying values of σ at $\alpha = 45°$. It is apparent that for $\bar{\gamma}$ in the neighborhood of 90°, increasing σ decreases $\bar{D}(\lambda)$. Hence, if we use an inversion of Eqn. 4 to calculate γ_0 for multilayers possessing the degree of mosaic spread determined by the X-ray diffraction experiments ($\sigma = 10°$—$20°$), it is obvious that the calculated range of $\gamma_0 = 72$—$90°$ is consistent with $\bar{\gamma} \simeq 90°$ where the thinner multilayers, which are known from the X-ray diffraction experiments to evidence lesser mosaic spread, have the higher dichroic ratios.

The individual values of γ_0 (and $\bar{\gamma}$) for both hemes *a* and a_3 are the subject of an accompanying paper [36].

(6) Nature of the EPR spectra

The EPR spectra from the frozen oriented multilayers of "membranous

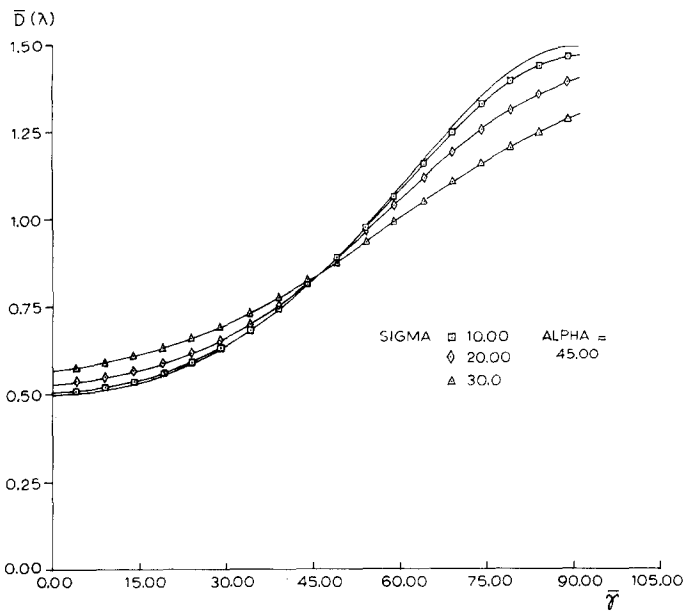

Fig. 5. $\bar{D}(\lambda)$ as a function of $\bar{\gamma}$ for different values of mosaic spread σ as calculated according to Eqn. 5. The values of σ are denoted in the figure by the various symbols; the solid line carrying no such symbol denotes $\sigma = 0°$.

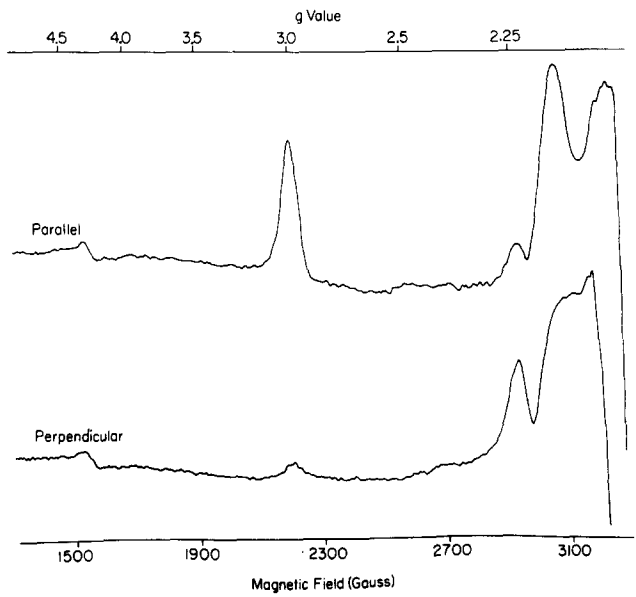

Fig. 6. EPR spectra of the oxidized cytochrome *c* oxidase in frozen oriented multilayers of "membranous cytochrome oxidase" where the plane of the multilayer is oriented parallel and normal (perpendicular) to the applied magnetic field. The oriented 1 cm diameter multilayer was formed from 6.5 mg protein (8.6 nmol heme *a*) of "membranous cytochrome oxidase" and the sample was partially dehydrated for 48 h at 4°C and 90% constant relative humidity. The partially dehydrated multilayer was cut with its mylar support into 2-mm strips which were inserted into the EPR capillary and frozen by immersion in liquid nitrogen. EPR frequency, 9.15 GHz; microwave power, 10 mW; sample temperature, 19.5°K. Scanning time, 2 min; time constant, 0.128 s. Modulation amplitude, 10 G.

cytochrome oxidase" at approx. 10°K are characteristic of low-spin heme resonances from oxidized cytochrome oxidase [37]. When the planes of the mylar supports are oriented parallel to the applied magnetic field, a resonance at g = 3 is maximal; when the planes of the mylar supports are oriented normal to the applied magnetic field, the amplitude of this resonance is virtually zero. The amplitude of the resonance at g = 2.2 shows precisely the converse dependence on the orientation of the applied magnetic field relative to the planes of the mylar supports. In addition the line-shapes are significantly different for these two resonances, the g = 3 resonance having an apparent "absorption" line-shape while the g = 2.2 resonance has the first-derivative of an "absorption" line-shape. See Fig. 6 for details of these results.

(7) Analysis of the EPR spectra

The g = 3 resonance from low-spin hemes corresponds to the z component of the low-spin heme g tensor g_z, i.e. that principal component of the g tensor along the direction normal to the heme plane [38]. The g = 2.2 resonance corresponds to the y component of the heme g tensor, g_y, i.e. a principal component of the g tensor lying in the heme plane. The resonance corresponding to the x component of the low-spin heme g tensor, g_x, at g = 1.5 was not investigated in these spectra.

Hence, the results reported in Section 6 above concerning the dependence of the g_z and g_y low-spin heme resonances on the orientation of the applied magnetic field relative to the plane of the frozen oriented multilayer of "membranous cytochrome oxidase" clearly indicate that the z-axis of the low-spin heme(s) responsible for these resonances must lie in the plane of the oriented multilayer.

The line-shapes of the g_z and g_y resonances are qualitatively explained in the following way: (a) The mosaic spread of these oriented multilayers would tend to average the first-derivative "single-crystal" line-shape for the g_z resonance to a considerable extent resulting in an apparent "absorption" line-shape because the g_z component occurs at an extremum of the heme g tensor, i.e. the magnitude of the g tensor varies relatively rapidly in the region about the principal z-axis. (b) Conversely, the mosaic spread of these multilayers would average the first derivative "single-crystal" line-shape for the g_y resonance to a relatively lesser extent which would tend to preserve its "single-crystal" character because the magnitude of the heme g tensor varies relatively less rapidly in the region about the principal y- (and x-) axis. The observed EPR spectra are presently being simulated using the mosaic spread determined from the X-ray diffraction experiments in order to more quantitatively account for the observed line-shapes of the various resonances; this study will be the subject of a future paper (Leigh, J.S., et al., work in progress).

Discussion

(1) Profile structure of the "membranous cytochrome oxidase" membrane

The low-resolution and "tentative" high-resolution unit cell electron density profiles shown in Figs. 2 and 3 clearly indicate the presence of two membranes within the average unit cell of the hydrated oriented multilayer. The electron

density profile for a single membrane is contained in the profile region $0 \leq x \leq D/2$ (and its mirror image is contained in the profile region $-D/2 \leq x \leq 0$) and possesses a rather high degree of asymmetry. The relatively higher electron density maxima at the surface of the membrane in the profile regions $x \approx 4$ Å and $x \approx 40$ Å and the relatively lower electron density minimum ($x \approx 13$ Å) in the interior of the membrane strongly suggests that a lipid bilayer forms the matrix of the membrane. The average electron density of the aqueous medium between the flattened vesicles in the profile region 60 Å $\leq x \leq D/2$ is similar to that of the relatively lower electron density minimum ($x \approx 13$ Å) in the interior of the membrane as shown most unambiguously in the low-resolution profile; this strongly suggests that the cytochrome oxidase molecules span the relatively lower electron density interior of the membrane since the interior of a lipid bilayer in the absence of incorporated protein would have a hydrocarbon chain interior whose average electron density would be considerably below that of an aqueous medium. The high degree of asymmetry in the single membrane profile indicates that the cytochrome oxidase molecules are all oriented similarly in the membrane profile with respect to "sidedness" properties of the membrane *. Finally, the resolution-limited narrow electron density maximum at the intravesicular surface of the membrane at $x \approx 4$ Å in the "tentative" high-resolution profile may arise from a well-localized layer of lipid polar headgroups in the profile projection; the extremely broad electron dense maximum at the extravesicular surface of the membrane extending over the profile region 12 Å $\leq x \leq 64$ Å in the "tentative" high-resolution profile is not likely to arise solely from the delocalization of lipid polar headgroups along the profile axis at this surface of the membrane, but must be at least partially due to a greater portion of the scattering mass of the oxidase molecule occurring within this region of the profile.

We note that our analysis cannot in principle distinguish between the unit cell electron density profiles $\rho(x)$ shown in Figs. 2 and 3 and their negative $-\rho(x)$ because $\rho(x)$ and $-\rho(x)$ have the same autocorrelation functions. However, the measured water content of these multilayers ($\approx 25\%$) strongly supports our choice of $\rho(x)$ as shown in Figs. 2 and 3 as the correct profiles where the regions 60 Å $\leq |x| \leq D/2$ would be identified with the aqueous spaces within the unit cell, the regions where swelling also occurs.

More precise determination of the extension of the oxidase molecule in the membrane profile and its profile structure are currently being investigated through a variation of the lipid/protein ratio of these membranes in the case of

* Conversely, if the "membranous cytochrome oxidase" vesicles did indeed possess random sidedness, the derived unit cell electron density profile would be expected to contain two rather symmetrical single membrane profiles (representing the symmetric portion of the single membrane profile) and the lamellar diffraction from the oriented multilayer should evidence the effects of substitution disorder arising from the anti-symmetric portion of the single membrane profile [31,39]. The substitution disorder phenomenon would evidence itself as a slowly varying incoherent lamellar intensity function underlying the coherent lamellar diffraction arising from the symmetric portion of the single membrane profile. Since the derived single membrane profile is highly asymmetric and since the minima of the coherent lamellar diffraction all approach the lamellar background scattering to within experimental error indicating the absence of any significant degree of substitution disorder in these multilayers, the large majority of cytochrome oxidase molecules are therefore oriented similarly in the membrane profile with respect to 'sidedness".

X-ray diffraction and through deuteration of the membrane's lipid component in the case of neutron diffraction.

We note that the magnitude of the lamellar X-ray diffraction relative to that of the equatorial diffraction from these hydrated oriented multilayers of "membranous cytochrome oxidase" strongly suggests that lamellar X-ray diffraction from oriented multilayers of the crystalline form of "membranous cytochrome oxidase" should be combined with the electron diffraction from tilted bilayers of the crystalline oxidase [12] in order to provide a complete three-dimensional structure for the cytochrome oxidase molecule.

(2) Planar structure of the "membranous cytochrome oxidase" membranes

The nature of the lower-angle equatorial diffraction arising from the distribution of cytochrome oxidase molecules in the plane of the membrane indicates that this planar distribution is certainly non-crystalline in our preparations and is probably similar to that of a planar liquid or real gas [40]. Upon binding cytochrome *c* to the "membranous cytochrome oxidase" in a 1 : 1 molar ratio with the oxidase, the planar distribution of oxidase molecules in the plane of these membranes in hydrated oriented multilayers becomes crystalline. The electron density profiles of such membranes in which the oxidase occurs in a planar lattice are somewhat different than those reported here; they indicate that cytochrome *c* is bound to the extravesicular surface of the membrane in agreement with our conclusions concerning the "sidedness" of these membranes. The detailed nature of the distribution of oxidase molecules in the plane of "membranous cytochrome oxidase" membranes and factors affecting that distribution are currently under investigation in our laboratory (Blasie, J.K., Erecińska, M., Wilson, D.F., Leigh, J.S. and Samuels, S., work in progress).

The nature of the "equatorial" diffraction in the region $s \approx 1/4.6$ Å indicates that the lipid fatty acid chains most likely occur in a highly-disordered melted state in these membranes [41].

(3) Internal structure of the cytochrome oxidase molecule

The strong equatorial diffraction in the region $s \approx 1/10$ Å and the strong meridional diffraction at $s \approx 1/5.2$ Å suggests the presence of bundles of α-helical polypeptide chains within the individual cytochrome oxidase molecules in which the average orientation of these α-helices is normal to the membrane plane. The equatorial diffraction at $s \approx 1/10$ Å would arise from interference effects between nearest neighbor α-helices in the bundle [40] (α-helical polypeptide chains having an effective diameter of $\approx$10 Å [42]) and the meridional diffraction at $s \approx 1/5.2$ Å would arise from the pitch of the α-helices [42].

Such secondary and tertiary structure for certain integral membrane proteins has been demonstrated previously for bacteriorhodopsin [43,44], vertebrate rhodopsin [45] and Ca^{2+}-ATPase from sarcoplasmic reticulum [29].

(4) Orientation of the cytochrome oxidase hemes relative to the membrane plane

The polarized optical and EPR spectroscopy on hydrated oriented multilayers of "membranous cytochrome oxidase" are consistent; these studies indi-

cate that the normal to the average heme plane lies essentially in the plane of the membrane. In accompanying papers [36,46], we present results which demonstrate that both the a and a_3 hemes of the cytochrome oxidase molecule have essentially this same orientation in these "membranous cytochrome oxidase" membranes and in the mitochondrial inner membrane.

Acknowledgement

This work was supported by an N.I.H. grant HL-18708 to M.E. and J.K.B.

References

1 Kuboyama, M., Yong, F.C. and King, T.E. (1972) J. Biol. Chem. 247, 6375—6383
2 Mason, T.L., Poyton, R.O., Whartan, D.C. and Schatz, G. (1973) J. Biol. Chem. 248, 1346—1354
3 Schwab, A.J., Sebald, W. and Weiss, H. (1972) Eur. J. Biochem. 30, 511—516
4 Rubin, M.S. and Tzagoloff, A. (1973) J. Biol. Chem. 248, 4269—4274
5 Lemberg, M.R. (1969) Physiol. Rev. 49, 48—121
6 Nicholls, P. and Chance, B. (1974) in Molecular Mechanisms of Oxygen Activation (Hayaishi, O., ed.), pp. 479—534, Academic Press, New York
7 Yonetani, T., Takemori, S., Sekuzu, I. and Okunuki, K. (1968) Nature 181, 1339—1340
8 Chuang, T.F., Sun, F.F. and Crane, F.L. (1970) J. Bioenerg. 1, 227—235
9 Sun, F.F., Prezbindowski, K.S., Crane, F.L. and Jacobs, E.E. (1968) Biochim. Biophys. Acta 153, 804—818
10 Jost, P.C., Griffith, O.H., Capaldi, R.A. and Vanderkooi, G. (1973) Proc. Natl. Acad. Sci. U.S. 70, 480—484
11 Vanderkooi, G., Senior, A.E., Capaldi, R.A. and Hayashi, H. (1972) Biochim. Biophys. Acta 274, 38—48
12 Henderson, R., Capaldi, R.A. and Leigh, Jr., J.S. (1977) J. Mol. Biol. 112, 631—648
13 Ruben, G.C., Telford, J.N. and Carroll, R.C. (1976) J. Cell Biol. 68, 724—739
14 Capaldi, R.A. (1973) Biochim. Biophys. Acta 303, 237—241
15 Racker, E., Burstein, C., Loyter, A. and Christiansen, O. (1970) in Electron Transport and Energy Conservation (Tager, J.M., Papa, S., Quagliariello, E. and Slater, E.C., eds.), pp. 235—252, Adriatica Editrice, Bari
16 Hackenbrock, C.R. and Miller-Hammon, K. (1975) J. Biol. Chem. 250, 9185—9197
17 Schneider, D.L., Kagawa, Y. and Racker, E. (1972) J. Biol. Chem. 247, 4074—4079
18 Eytan, G.D., Carroll, R.C., Schatz, G. and Racker, E. (1975) J. Biol. Chem. 250, 8598—8603
19 Junge, W. and de Vault, D. (1975) Biochim. Biophys. Acta 408, 200—214
20 Blasie, J.K., Erecińska, M., Leigh, J.S. and Samuels, S. (1977) Biophys. J. 17, 63a
21 Erecińska, M., Oshino, R., Oshino, N. and Chance, B. (1973) Arch. Biochem. Biophys. 157, 431—445
22 Garnall, A.G., Bardawill, C.J. and David, M.M. (1949) J. Biol. Chem. 177, 751—766
23 Bartlett, G.R. (1959) J. Biol. Chem. 234, 466—468
24 Wilson, D.F. and Dutton, P.L. (1970) Arch. Biochem. Biophys. 136, 583—584
25 Dutton, P.L. (1971) Biochim. Biophys. Acta 226, 63—80
26 Laemmli, U. (1970) Nature 227, 680—684
27 Blasie, J.K. (1972) Biophys. J. 12, 191—204
28 Gabriel, A. and Dupont, Y. (1972) Rev. Sci. Instrum. 43, 1600
29 Herbette, L., Marquardt, J., Scarpa, A. and Blasie, J.K. (1977) Biophys. J., in the press
30 Erecińska, M., Blasie, J.K. and Wilson, D.F. (1977) FEBS Lett. 76, 235—239
31 Schwartz, S., Cain, J.E., Dratz, E. and Blasie, J.K. (1975) Biophys. J. 15, 1201—1233
32 Lesslauer, W. and Blasie, J.K. (1971) Acta Cryst. A27, 456—461
33 Adar, F., The Porphyrins (Dolphin, D., ed.)
34 Cherry, R.J., Hsu, K. and Chapman, D. (1972) Biochim. Biophys. Acta 267, 512—525
35 Born, M. and Wolff, E. (1964) Principles of Optics, The Macmillan Co., New York
36 Erecińska, M., Wilson, D.F. and Blasie, J.K. (1978) Biochim. Biophys. Acta 501, 53—62
37 Hartzell, C.R. and Beinert, H. (1974) Biochim. Biophys. Acta 368, 318—338
38 Mailer, C. and Taylor, C.P.S. (1972) Can. J. Biochem. 50, 1048—1055
39 Cain, J. (1974) Ph.D. Thesis, University of Pennsylvania
40 James, R.W. (1965) in The Crystalline State (Sir Lawrence Bragg, ed.) Vol. II, Cornell University Press, Ithaca
41 Engelman, D.M. (1975) Biophys. J. 15, 940—944
42 Pauling, L. and Corey, R.B. (1953) Nature 171, 59—61
43 Henderson, R. (1975) J. Mol. Biol. 93, 123—138
44 Blaurock, A.E. (1975) J. Mol. Biol. 93, 139—158
45 Santillan, G. (1975) Ph.D. Thesis, University of Pennsylvania
46 Erecińska, M., Wilson, D.F. and Blasie, J.K. (1978) Biochim. Biophys. Acta 501, 63—71